RAA 2016 Vol. **16** No. **1**, 17 (6pp) doi: 10.1088/1674–4527/16/1/017
http://www.raa-journal.org *http://iopscience.iop.org/raa*

Research in Astronomy and Astrophysics

Mode coupling in solar spicule oscillations

Zahra Fazel

Astrophysics Department, Physics Faculty, University of Tabriz, Tabriz, Iran; *z_fazel@tabrizu.ac.ir*

Received 2015 July 13; accepted 2015 November 8

Abstract In a real medium which has oscillations, the perturbations can cause an energy transfer between different modes. A perturbation, which is interpreted as an interaction between the modes, is inferred to be mode coupling. The mode coupling process in an inhomogeneous medium such as solar spicules may lead to the coupling of kink waves to local Alfvén waves. This coupling occurs in practically any conditions when there is smooth variation in density in the radial direction. This process is seen as the decay of transverse kink waves in the medium. To study the damping of kink waves due to mode coupling, a 2.5-dimensional numerical simulation of the initial wave is considered in spicules. The initial perturbation is assumed to be in a plane perpendicular to the spicule axis. The considered kink wave is a standing wave which shows an exponential damping in the inhomogeneous layer after the mode coupling occurs.

Key words: solar spicules — mode coupling — MHD waves

1 INTRODUCTION

Spicules are one of the important phenomena in the solar chromosphere which are observed at the limb (Zaqarashvili & Erdélyi 2009). In order to study the oscillations in spicules, many works have been done observationally and theoretically (De Pontieu et al. 2004; Kukhianidze et al. 2006; Kuridze et al. 2013; Verth et al. 2011). The generation and propagation of magnetohydrodynamic (MHD) waves in the interval of the spicule lifetime (about $5-15$ min) can be detected by spicule observations.

Helioseismology can determine the properties of solar phenomena from observed oscillations, an idea which was originally suggested by Zaqarashvili et al. (2007) for chromospheric spicules (Verth et al. 2011). By estimating the period of oscillations, two types of MHD waves are observed in spicules: kink waves (Nikolsky & Platova 1971; De Pontieu et al. 2007; He et al. 2009; Ebadi et al. 2012) and Alfvén waves reported by Jess et al. (2009). Since spicules are denser than surrounding coronal plasma (Beckers 1968), they can be modeled as cool magnetic tubes embedded in hot coronal plasma.

Damping of MHD waves (kink or Alfvén waves) can be considered as a mechanism that leads to solar coronal heating. When MHD waves interact with plasma inhomogeneities, a number of physical phenomena are generated such as resonant absorption, mode coupling, phase mixing, and wave dispersion.

The process of conversion of energy from the incompressible kink mode to an Alfvén wave describes mode coupling in an inhomogeneous medium. This process can take place in each oscillating phenomenon. For example in sunspots, it takes place between the p-mode seismic wave field of the solar interior and the oscillations in the overlying atmosphere (conversion of fast to slow modes) (Cally et al. 1994). Pascoe et al. (2010) have studied the damping of kink waves due to mode coupling in solar coronal loops. They have demonstrated that the observed loop displacements are the coupled kink-Alfvén waves, i.e. transverse footpoint motions travel along the loop and couple to Alfven waves through the inhomogeneity at the loop boundary. When an inhomogeneous layer in encountered, the Alfvén speed varies continuously and resonant absorption occurs where the phase speed of the kink wave matches the local Alfvén wave speed ($C_k = V_{\rm A}(r)$) (Allan & Wright 2000; Hood et al. 2013). Terradas et al. (2010) demonstrated that the damping of the transverse motions through mode coupling is frequency dependent. Using the CoMP data (Tomczyk & McIntosh 2009), Verth et al. (2010) found evidence for this frequency that strengthens the interpretation in which the observed propagating Doppler shift oscillations are the coupled kink-Alfvén waves.

Here, we study the damping of the observed transverse oscillations of the solar spicule axis. This study is referring to the results obtained by analyzing the time series of the Ca II H-line obtained from Hinode/SOT on the solar limb (Tsuneta et al. 2008). These observed transverse oscillations were interpreted as standing kink waves (Ebadi et al. 2012). This paper is organized as follows. The basic equations and theoretical model are presented in Section 2. In Section 3, numerical results are presented and discussed, and Section 4 contains the conclusion.

2 BASIC EQUATIONS OF THE MODEL

The damping of standing kink waves is studied in a spicule environment through the mode coupling mechanism. We perform a 2.5-dimensional simulation of MHD equations in a stratified medium. Non-ideal MHD equations in the plasma dynamics are as follows:

$$\frac{\partial \boldsymbol{\rho}}{\partial t} + \nabla \cdot (\rho \boldsymbol{V}) = 0\,, \tag{1}$$

$$\rho \frac{\partial \boldsymbol{V}}{\partial t} + \rho(\boldsymbol{V}\cdot\nabla)\boldsymbol{V} = -\nabla p + \rho \boldsymbol{g} + \frac{1}{\mu_0}(\nabla \times \boldsymbol{B}) \times \boldsymbol{B} + \rho\nu\nabla^2 \boldsymbol{V}\,, \tag{2}$$

$$\frac{\partial \boldsymbol{B}}{\partial t} = \nabla \times (\boldsymbol{V} \times \boldsymbol{B}), \nabla \cdot \boldsymbol{B} = 0\,, \tag{3}$$

$$\frac{\partial p}{\partial t} + \nabla \cdot (p\boldsymbol{V}) = (1-\gamma) p \nabla \cdot \boldsymbol{V}\,, \tag{4}$$

where $p = \rho RT/\mu$ is the pressure for a perfect gas, ρ is the plasma density, μ is the mean molecular weight, μ_0 is the vacuum permeability, ν is a constant viscosity coefficient, $\gamma = 5/3$ is the adiabatic index, and g is the gravitational acceleration. We apply $\rho\nu = 2.2\times10^{-17} T^{5/2}$ kg m^{-1} s^{-1} to a fully ionized hydrogen plasma (Priest 1982).

2.1 The Equilibrium State

Vectors $\boldsymbol{V}$ and $\boldsymbol{B}$ in Equations (1)–(4) are the velocity and magnetic field respectively which are defined as follows:

$$\begin{aligned} \boldsymbol{V} &= \boldsymbol{v}_0 + \boldsymbol{v}\,, \\ \boldsymbol{B} &= \boldsymbol{B}_0 + \boldsymbol{b}\,, \end{aligned} \tag{5}$$

where $\boldsymbol{v}_0 = v_0\hat{k}$ and $\boldsymbol{B}_0$ are the equilibrium velocity and magnetic field respectively. In order to have the kink waves coupled with Alfvén waves, an equilibrium magnetic field is considered to be $\boldsymbol{B}_0 = B_0(\alpha\hat{j} + \hat{k})$ where α is a constant value ($\alpha < 1$). In this case, the y-component of the magnetic field is smaller than its z-component by a factor of α. Since the equilibrium magnetic field is force-free, the pressure gradient is balanced by the gravity force via equation $-\nabla p_0(x,z) + \rho_0(x,z)\boldsymbol{g} = 0$, where $\boldsymbol{g} = (0,0,-g)$, and the pressure in an equilibrium state is described by

$$p_0(x,z) = p_0(x)\ \exp(-z/H)\,. \tag{6}$$

Since coupling between kink and Alfvén waves occurs in practically any conditions when there are smooth density variations in the radial direction (here, the x-direction) (Ruderman & Roberts 2002; Soler et al. 2011), the density profile is written in the following form

$$\rho_0(x,z) = \rho_0(x)\ \exp(-z/H)\,, \tag{7}$$

where $H = \frac{RT}{\mu g}$ is the pressure scale height and the atmosphere is considered isothermal. Also, $\rho_0(x)$ is considered to be the following (De Moortel et al. 1999; Ruderman & Roberts 2002; Karami & Ebrahimi 2009)

$$\rho_0(x) = \frac{1}{2}\rho_0\Big[1 + d_\rho - (1-d_\rho)\tanh((x-1)/d)\Big]\,, \tag{8}$$

where $d_\rho = \frac{\rho_e}{\rho_0} = 0.01$. Here ρ_0 is the plasma density in the spicule, ρ_e is the external density, and d is the width of the inhomogeneous layer.

2.2 Perturbation Equations

In order to make continuous displacements of the tube axis of a spicule, a perturbation in the velocity and magnetic field is considered at the lower boundary of the tube. Vectors $\boldsymbol{v}$ and $\boldsymbol{b}$ in Equation (5) are the perturbed velocity and magnetic field which are defined as $\boldsymbol{v} = (v_x, v_y, v_z)$ and $\boldsymbol{b} = (b_x, b_y, b_z)$, respectively. The initial perturbed velocity is considered to have a two dimensional dipole form as introduced by Pascoe et al. (2010):

$$\begin{aligned} v_x(x,z,t=0) &= \frac{x^2 - z^2}{(x^2+z^2)^2}\,, \\ v_y(x,z,t=0) &= \frac{2xz}{(x^2+z^2)^2}\,, \\ v_z(x,z,t=0) &= A_v \sin(\pi x)\sin(\pi z)\,, \end{aligned} \tag{9}$$

and

$$\begin{aligned} (b_x, b_y, b_z)(x,z,t=0) &= A_b \sin(\pi x)\sin(\pi z)\,, \\ p(x,z,t=0) &= A_p \sin(\pi x)\sin(\pi z)\,, \end{aligned} \tag{10}$$

where A_v, A_b and A_p are the small amplitudes of the perturbed velocity, magnetic field and pressure respectively (by choosing these small amplitudes, the components tend to be almost zero. These choices are made to avoid some unwanted effects in our simulation code).

In order to see the variations of the perturbed velocity and magnetic field, linearized dimensionless MHD equations with the considered assumptions are as follows:

$$\begin{aligned} \frac{\partial v_x}{\partial t} + v_0\frac{\partial v_x}{\partial z} &= \frac{1}{\rho_0(x,z)}\Big(\frac{\partial b_x}{\partial z} - \alpha\frac{\partial b_y}{\partial x} - \frac{\partial b_z}{\partial z}\Big) + \nu\nabla^2 v_x\,, \\ \frac{\partial v_y}{\partial t} + v_0\frac{\partial v_y}{\partial z} &= \frac{1}{\rho_0(x,z)}\frac{\partial b_y}{\partial z} + \nu\nabla^2 v_y\,, \\ \frac{\partial v_z}{\partial t} + v_0\frac{\partial v_z}{\partial z} &= -\beta\frac{\partial P}{\partial z} - g + \frac{\alpha}{\rho_0(x,z)}\frac{\partial b_y}{\partial z} + \nu\nabla^2 v_z\,, \end{aligned} \tag{11}$$

$$\begin{aligned} \frac{\partial b_x}{\partial t} &= \frac{\partial v_x}{\partial z} - v_0\frac{\partial b_x}{\partial z}\,, \\ \frac{\partial b_y}{\partial t} &= \frac{\partial v_y}{\partial z} - v_0\frac{\partial b_y}{\partial z}\,, \\ \frac{\partial b_z}{\partial t} &= \frac{\partial v_z}{\partial z} - v_0\frac{\partial b_z}{\partial z}\,, \end{aligned} \tag{12}$$

where $\beta(z) = \frac{p_0(z)}{B_0^2/2\mu}$ is the ratio of gas pressure to magnetic pressure. The boundary conditions for a standing formalism are defined to be $\boldsymbol{v} = 0$ and $\boldsymbol{b} = 0$ at $z = 0$ and L. Hence by considering these conditions in Equation (4), we have $p = 0$ at boundaries $z = 0$ and L (Ruderman & Roberts 2002).

3 DISCUSSION

In order to solve the coupled Equations (11) and (12) numerically, the finite difference and fourth-order Runge-Kutta methods are used to calculate the space and time derivatives, respectively. The implemented numerical scheme relies on the forward finite difference method to take the first spatial derivatives with a truncation error of (Δx), which is the spatial resolution in the x direction. The order of approximation for the second spatial derivative in the finite difference method is $O((\Delta x)^2)$. On the other hand, the fourth-order Runge-Kutta method takes the time derivatives into account. The computational output data are given to an accuracy of 17 decimal digits (Fazel & Ebadi 2014). We set the number of mesh-grid points as 256×256. The time step is chosen as 0.0001, and the system length in the x and z dimensions (simulation box sizes) are set to be $(0, 4)$ and $(0, 20)$ respectively.

In the considered conditions for a spicule, the values of all the presented parameters are (Murawski & Zaqarashvili 2010, Ebadi et al. 2012, Fazel & Ebadi 2013): $L = 6000$ km (spicule length), $a = 250$ km (spicule radius), $d = 0.2a = 50$ km (inhomogeneous layer width), $n_e = 11.5 \times 10^{16}$ m^{-3}, $V_{A0} = 50$ km s^{-1}, $v_0 = 25$ km s^{-1}, $B_0 = 1.2 \times 10^{-3}$ Tesla, $T_0 = 14\ 000$ K, $p_0 = 3.7 \times 10^{-2}$ N m^{-2}, $\rho_0 = 1.9 \times 10^{-10}$ kg m^{-3}, $g = 272$ m s^{-2}, $R = 8300$ m^{2}s^{-1}k^{-1} (universal gas constant), $H = 750$ km, $\mu = 0.6$, $\mu_0 = 4\pi \times 10^{-7}$ Tesla m A^{-1}, $\tau = a/C_k = 5$ s (the period of oscillations), and $A_v = A_b = A_p = 10^{-8}$ (dimensionless amplitudes of perturbed velocity, magnetic field and pressure respectively).

Considering Equations (11) and (12), the y-component of the velocity and magnetic field define the y-independent Alfvén waves. By rewriting the y-component of these equations and by combining them, we can obtain

$$\rho_0\Big[\frac{\partial^2 v_y}{\partial t^2} + (\boldsymbol{v}_0\cdot\nabla)\frac{\partial v_y}{\partial t}\Big] = \frac{1}{\mu_0}\Big[(\boldsymbol{B}_0\cdot\nabla)^2 v_y - (\boldsymbol{v}_0\cdot\nabla)b_y\Big] + \rho_0\nu\nabla^2\frac{\partial v_y}{\partial t}. \quad (13)$$

This equation describes the damped Alfvén waves that have velocity and magnetic field perturbations in the y-direction and propagate along the equilibrium magnetic field. If for a moment we forget about ν and adopt a local analysis, the dispersion relation is obtained as $\sigma^2 = \frac{k_\parallel^2 B_0^2}{\rho_0} = k_\parallel^2 V_{\rm A}^2$, where $k_\parallel = \alpha k_y + k_z$ is the parallel wave number and $V_{\rm A}$ is the local Alfvén velocity. The second row of Equations (11) and (12) describes the damped Alfvén waves which are coupled with the first and third rows of Equations (11) and (12). The equations tell us that a transfer of energy from motions described by the variables (v_x, v_z, b_x, b_z) to motions described by the variables (v_y, b_y) can occur in the considered MHD waves. The variables (v_x, v_z, b_x, b_z) are damped due to the coupling to Alfvén waves. These results are demonstrated in the following figures for the perturbed velocity and magnetic field variations.

At $t = 0$, the initial perturbation is applied at the lower z boundary. This perturbation uniformly propagates upward and then it stops at the upper z boundary (the standing case).

Figure 1 is the plot of the initial wave packet given by Equation (9). In the case of an inhomogeneous layer ($\rho_0/\rho_e > 1$), since the initial perturbation acts over all density regions (inside the spicule, in the inhomogeneous layer and outside the spicule), the Alfvén speed varies in these regions ($V_{\rm A}(x, z)$). The Alfvén speed varies continuously in the inhomogeneous layer and resonant absorption occurs where the condition $v_{\rm A} = v_{\rm phase}$ is satisfied. Here, $v_{\rm phase} = \omega/k_z$, where ω is the angular frequency of kink oscillation and k_z is the local longitudinal wave number. In our simulation, the spicule is considered to be a thin flux tube ($a = 250$ km radius) with a thin inhomogeneous layer ($d = 0.2a = 50$ km width). In this approach, the above condition is satisfied in the considered inhomogeneous layer, so this is the reason that mode coupling occurs in the modeled spicule.

Figure 2 shows the perturbed velocity variations of v_x with respect to z (height or propagation direction) at $t = 10\tau$ s (top panel) and $t = 40\tau$ s (bottom panel). The perturbed velocity is normalized to V_{A0}. At $t = 10\tau$ s, the perturbed v_x already shows damping due to phase mixing occurring in the inhomogeneous layer. By the later stage at $t = 40\tau$ s, we see that the initial perturbation (the kink wave) has undergone a complete attenuation and only the phase-mixed Alfvén wave with bigger amplitude remains in the layer. The lower panel shows an exponential damping of v_x with z. This is in good agreement with results obtained by Pascoe et al. (2012). They have demonstrated that for standing kink modes with the approximations of a thin flux tube and thin boundary layer, an exponential damping envelope is obtained. In both panels at the first heights, the total amplitude of velocity oscillations has values near the initial ones. As height increases, the perturbed velocity amplitude decreases to smaller values which demonstrates the damping process occurs due to mode coupling. The coupling of the kink wave to a local Alfvén mode causes a decrease in wave energy in the spicule, and so appears to dampen the spicule oscillation.

Figure 3 shows the three-dimensional (3D) plots of the perturbed velocity in the $x - z$ space at two time steps (as mentioned in Fig. 2).

Figure 4 demonstrates variations of the perturbed magnetic field component, b_x, with respect to z at two locations: the spicule axis (according to our simulation box, the spicule axis is placed at the dimensionless point $x = 2$ corresponding to $x = 250$ km) (upper panel), and inhomogeneous layer ($x = 3.8$ corresponding to $x = 475$ km) (lower panel). The upper panel shows the upwards propagating kink oscillations (with smaller amplitude) along the spicule axis which undergoes damping due to mode coupling as height increases. The lower panel shows the Alfvén mode (with bigger amplitude) in the inhomoge-

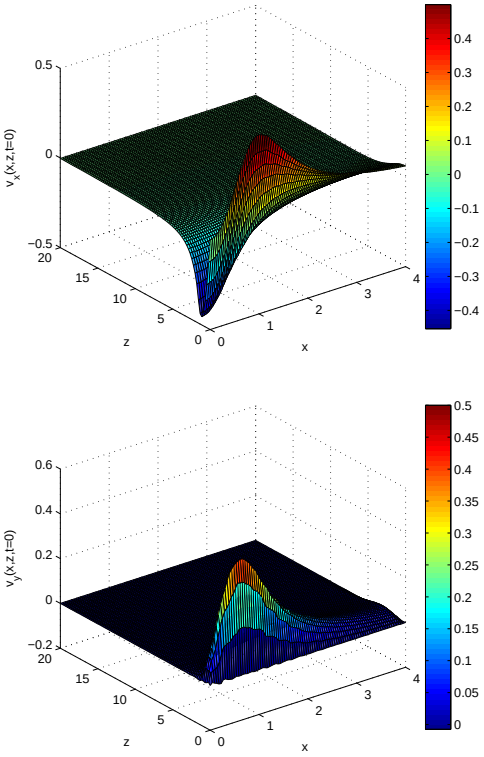

Fig. 1 The initial wave packet (v_x and v_y) is shown at $t = 0$ s.

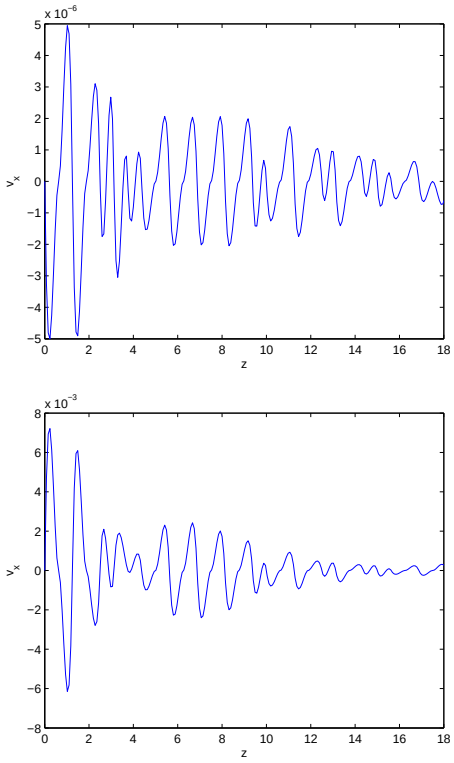

Fig. 2 The perturbed velocity variations are shown with respect to z at two time steps: $t = 10\tau$ s (*top panel*) and $t = 40\tau$ s (*bottom panel*).

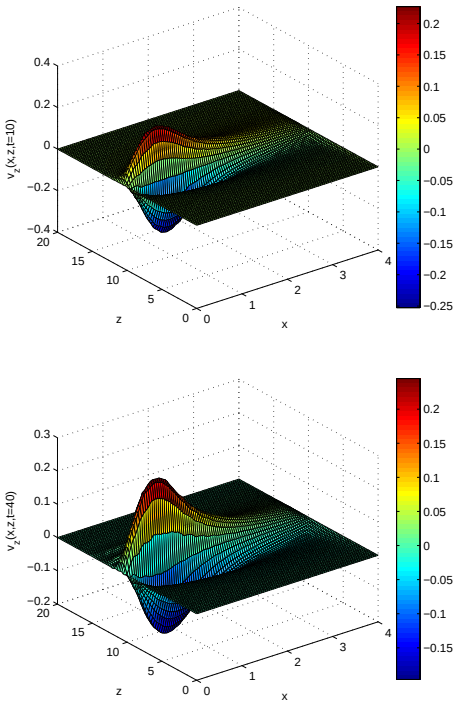

Fig. 3 The perturbed velocity in $x - z$ space is shown. The top panel corresponds to $t = 10\tau$ s and the bottom panel to $t = 40\tau$ s.

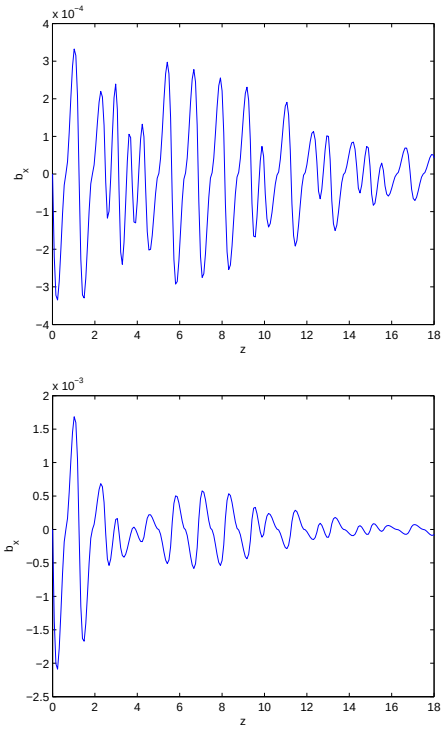

Fig. 4 The perturbed magnetic field (b_x) variations are shown with respect to z. The top panel shows the kink mode along the spicule axis at $x = 250$ km. The bottom panel shows the Alfvén mode in the inhomogeneous layer at $x = 475$ km. The perturbed magnetic fields are normalized to B_0.

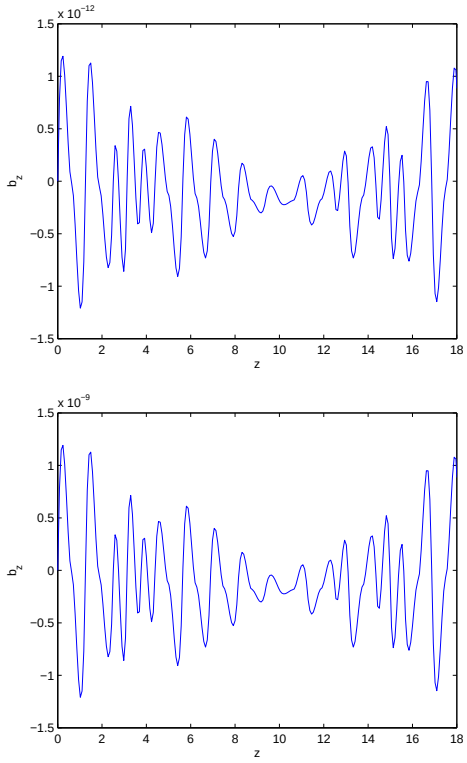

Fig. 5 The perturbed magnetic field (b_z) variations are shown with respect to z. The top panel shows the kink mode along the spicule axis. The bottom panel shows the Alfvén mode in the inhomogeneous layer. The perturbed magnetic fields are normalized to B_0.

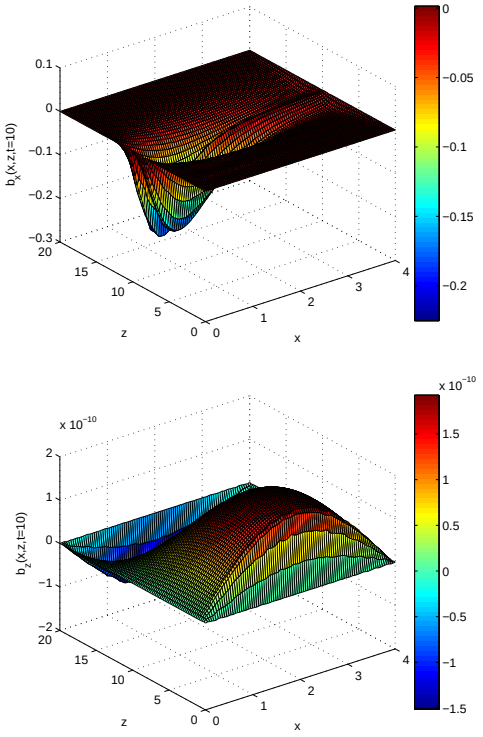

Fig. 6 The perturbed magnetic field is shown in $x-z$ space at $t = 10\tau$ s.

neous layer. The component b_x grows in z as energy is transferred to the Alfvén mode from the kink mode.

Figure 5 demonstrates variations of the perturbed magnetic field component, b_z, with respect to z at the same locations as in Figure 4. The component b_z has small fluctuations which indicate an almost incompressible kink mode in the inhomogeneous layer (with an amplitude of about 10^{-9}).

The 3D plots of the perturbed magnetic field components with respect to x and z are presented in Figures 6 (at $t = 10\tau$ s) and 7 (at $t = 40\tau$ s). In these figures, the spatial damping of the oscillations is also seen along the tube axis.

In Figure 8, the total energy normalized to the initial total energy is presented. The wave energy is defined as $E_{\rm tot} = 1/2(\rho(v_x^2 + v_y^2 + v_z^2) + 1/\mu(b_x^2 + b_y^2 + b_z^2))$. The coupling of the kink mode to the local Alfvén mode leads to a decrease in the kink wave energy in the spicule which is exhibited as damping of the tube oscillations. The amplitude of total energy decreases exponentially with time. The period of the kink waves ($P_k = 2L/C_k = 241.2$ s) is in good agreement with spicule lifetimes ($5 - 15$ min) (Zaqarashvili & Erdélyi 2009).

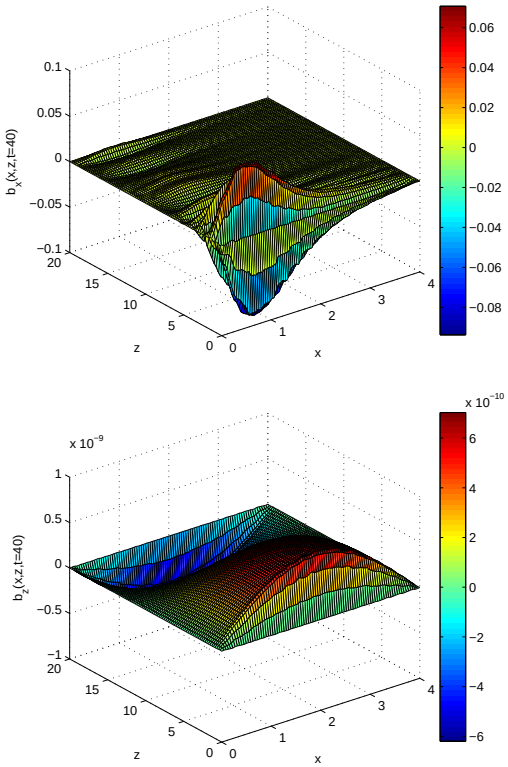

Fig. 7 The perturbed magnetic field is shown in $x-z$ space at $t = 40\tau$ s.

4 CONCLUSIONS

In this paper, we attempt to investigate the behavior of MHD waves observed in solar spicules. The purpose is to

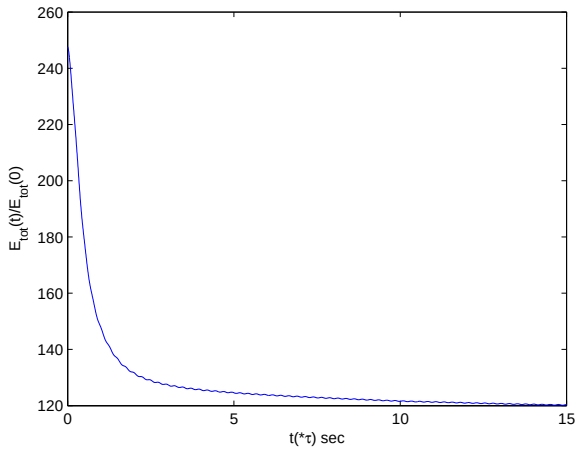

Fig. 8 Time variations of the total energy are presented.

study their damping process by a mode coupling mechanism. To do this, a typical spicule is considered to be a thin flux tube in the $x-z$ plane, and an initial perturbation is assumed as a transverse kink wave at the lower z-boundary of the tube. An initial perturbation is applied to the velocity and the magnetic field of the spicule, which leads to transverse displacement of the spicule axis. These transverse waves undergo a damping due to plasma inhomogeneity as height increases in which an energy transfer takes place from the kink mode to the local Alfvén mode. The amplitude of the Alfvén wave grows along the tube axis, and then experiences a spatial damping in the spicule. We observe that the total energy of the coupled kink to Alfvén waves decreases with time exponentially.

In the approach of modeling a spicule using a thin tube with a thin inhomogeneous layer, the dissipation takes place in this layer around $V_{\rm A} = C_k$ where $C_k = \sqrt{(\frac{1}{1+\rho_e/\rho_0})}V_{A0}$ (Kukhianidze et al. 2006). The exponential damping of the spicule oscillations gives a damping time which depends on the period of oscillation and the spicule parameters (Pascoe et al. 2012). The obtained $\tau_{\rm damp} = 8.5$ min is in good agreement with the spicule lifetime. This simulation is based on observational results reported by Ebadi et al. (2012). They studied these oscillations observationally and theoretically, and analyzed the time series of the Ca II H-line obtained from Hinode/SOT on the solar limb. The time distance analysis shows that the axis of a spicule undergoes quasi-periodic transverse displacement at different heights from the photosphere. The theoretical analysis also shows that the observed oscillations may correspond to the fundamental harmonic of standing kink waves.

In this case, our initial perturbation corresponds to some general photospheric motion and our kink waves correspond to the transverse oscillations in the spicule axis observed from Hinode/SOT by Tsuneta et al. (2008).

References

Allan, W., & Wright, A. N. 2000, J. Geophys. Res., 105, 317
Beckers, J. M. 1968, Sol. Phys., 3, 367
Cally, P. S., Bogdan, T. J., & Zweibel, E. G. 1994, ApJ, 437, 505
De Moortel, I., Hood, A. W., Ireland, J., & Arber, T. D. 1999, A&A, 346, 641
De Pontieu, B., Erdélyi, R., & James, S. P. 2004, Nature, 430, 536
De Pontieu, B., McIntosh, S. W., Carlsson, M., et al. 2007, Science, 318, 1574
Ebadi, H., Zaqarashvili, T. V., & Zhelyazkov, I. 2012, Ap&SS, 337, 33
Fazel, Z., & Ebadi, H. 2013, Ap&SS, 346, 319
Fazel, Z., & Ebadi, H. 2014, Ap&SS, 350, 57
He, J., Marsch, E., Tu, C., & Tian, H. 2009, ApJ, 705, L217
Hood, A. W., Ruderman, M., Pascoe, D. J., et al. 2013, A&A, 551, A39
Jess, D. B., Mathioudakis, M., Erdélyi, R., et al. 2009, Science, 323, 1582
Karami, K., & Ebrahimi, Z. 2009, PASA, 26, 448
Kukhianidze, V., Zaqarashvili, T. V., & Khutsishvili, E. 2006, A&A, 449, L35
Kuridze, D., Verth, G., Mathioudakis, M., et al. 2013, ApJ, 779, 82
Murawski, K., & Zaqarashvili, T. V. 2010, A&A, 519, A8
Nikolsky, G. M., & Platova, A. G. 1971, Sol. Phys., 18, 403
Pascoe, D. J., Wright, A. N., & De Moortel, I. 2010, ApJ, 711, 990
Pascoe, D. J., Hood, A. W., de Moortel, I., & Wright, A. N. 2012, A&A, 539, A37
Priest, E. R. 1982, Solar Magneto-Hydrodynamics (Dordrecht, Holland; Boston : D. Reidel Pub. Co.; Hingham)
Ruderman, M. S., & Roberts, B. 2002, ApJ, 577, 475
Soler, R., Terradas, J., Verth, G., & Goossens, M. 2011, ApJ, 736, 10
Terradas, J., Goossens, M., & Verth, G. 2010, A&A, 524, A23
Tomczyk, S., & McIntosh, S. W. 2009, ApJ, 697, 1384
Tsuneta, S., Ichimoto, K., Katsukawa, Y., et al. 2008, Sol. Phys., 249, 167
Verth, G., Goossens, M., & He, J.-S. 2011, ApJ, 733, L15
Verth, G., Terradas, J., & Goossens, M. 2010, ApJ, 718, L102
Zaqarashvili, T. V., & Erdélyi, R. 2009, Space Sci. Rev., 149, 355
Zaqarashvili, T. V., Khutsishvili, E., Kukhianidze, V., & Ramishvili, G. 2007, A&A, 474, 627